Horizontal Variability of Microstructure in the Vicinity of a Sargasso Sea Front

G. O. MARMORINO, J. P. DUGAN* AND T. E. EVANS**

Marine Technology Division, Code 5810, Ocean Dynamics Branch, Naval Research Laboratory, Washington, DC 20375

(Manuscript received 27 February 1985, in final form 9 December 1985)

ABSTRACT

Temperature microstructure variability has been determined from measurements of electrical conductivity (~1.5 cm wavelength resolution) along two depths in the seasonal thermocline of the Sargasso Sea in July 1981. The microstructure sensors were attached to a thermistor chain, which was towed in and away from a frontal shear zone in the region of the Subtropical Convergence Zone. Averaged over the 170-km-long tow, the estimated dissipation rate of temperature variance, χ, was $\sim 10^{-8}$ °C^2 s^{-1}, but χ values ranged from 10^{-11} (noise level) to 10^{-5} in the most energetic events. Cox numbers, C, were calculated by making use of a local temperature gradient calculated over a fixed ~1 m vertical spacing on the chain. Mean values of C were ~10, but values as high as 10^5 were observed. The signals were highly intermittent, varying by as much as five orders of magnitude over scales of the order of 10 m. Probability distributions of χ and C appeared to resemble the lognormal form only in cases where the data were carefully drawn from energetic events. Low values of a large-scale Richardson number (7 m vertical by 450 m horizontal averages) bore no consistent relationship to the occurrence of an event.

1. Introduction

An important question in physical oceanography is the nature of the link between small-scale mixing processes and large-scale dynamics. One expects this link to be most clear in localized regions of high kinetic energy or high shear such as in rings and density fronts or at the base of the surface mixed layer. The problem confronting the microstructure worker is that a prodigious amount of microstructure sampling may be required to adequately measure the dissipation rates in the mixing events and to ascertain the degree to which a given region is statistically homogeneous with respect to the turbulence (Caldwell, 1983; Gibson, 1982).

Recent attempts at exploring the horizontal variability of the mixing have used a towed conductivity sensor system (Washburn and Gibson, 1982; 1984); and, although their instrument noise level was very high, Washburn and Gibson (1984) attempt to make statistically reliable estimates of mixing rates below the base of the mixed layer during the Mixed Layer Experiment (MILE). They estimate a lognormal distribution from their data, and infer that the mode of the distribution is consistent with nearby microstructure profiler measurements, while the mean is considerably higher. That the distribution function is generally non-Gaussian is well documented (e.g., Gregg, 1980), but its particular form might or might not be lognormal, and the extrapolation of the mode and mean to values well below the system noise level is fraught with uncertainty.

Microstructure work in a region of strong shear includes that of Oakey and Elliott (1977). Their measurements with a dropped profiler in the region of the Gulf Stream yielded a correlation between microstructure and finestructure variance, but they could extract no clear dynamical relationship to mixing intensity. Gregg and Sanford (1980) found microstructure activity in the Gulf Stream to be dominated by double diffusion occurring on the boundaries of thermohaline intrusions, and they suggest that much of the activity measured by Oakey and Elliott was of a similar nature. Gargett (1978) also found microstructure concentrated at boundaries of intrusive features, presumably of frontal origin. Away from the salt-stabilized temperature inversions, Gregg and Sanford found low microstructure levels, yielding Cox numbers of only about 50 in the high-shear zone. However, they allow for the possibility that the energetic events were missed because of the small number (only five) of vertical profiles. From nearly simultaneous shear profiles they calculated Richardson numbers over 50-m depth bins, but found

* Present Affiliation: Arete Associates, Arlington, VA 22215.
** Permanent Address: 3229 Military Road NW, Washington, DC 20015.

no consistent relationship between Cox and Richardson numbers.

In this paper, microstructure measurements are presented that were obtained along two depths in a long (170 km) tow with a thermistor chain in the vicinity of an upper ocean density front in the Sargasso Sea, in the region of the Subtropical Convergence Zone. Like Washburn and Gibson, high-frequency response conductivity sensors were used to measure conductivity variance, from which we infer (as they did) the temperature variance. By combining these measurements with simultaneous observations of the local vertical temperature gradient, the horizontal variation of mixing activity (the Cox number) is determined as well. Fluctuations on scales smaller than about 1.5 cm were not resolved by the probes, so the variance was not fully accounted for in the more energetic events; thus, mixing intensities and dissipation values are underestimated to some unknown extent.

Marmorino et al. (1985, hereafter MRDS) have already explored the spatial variability of temperature finestructure (1 to 3 m horizontal wavelengths) in the two frontal crossings contained in the present, longer dataset (Fig. 1); the reader is referred to that paper for additional details about the experiment. Their main results were that spatially coherent "patches" of elevated levels of finestructure occur most extensively in the frontal zone, where coarse-scale estimates of the Richardson number are lowest; that features in the temperature field within the larger patches are suggestive of overturning internal waves; and that the resolved patches do not show any consistent pattern with respect to features suggestive of intrusions, such as temperature inversion zones. This all suggested that shear instabilities were an important mechanism. Like Oakey and Elliott, they also found that the finestructure and microstructure signals were correlated and, so, the finescale variability is plausibly related to mixing variability, but there were wide variations (over four decades) in the ratio of the two signals, prohibiting reliable estimation of mixing parameters from the finestructure results alone.

The present paper is arranged as follows. Section 2 discusses the instrumentation. Two independent sensors were used to discriminate between microstructure and spurious signals (particulate spikes and biological fouling of the probes). Section 3 discusses the assumptions used in analysis and their shortcomings. The results are given in section 4. Of particular interest is the signal's spatial distribution, intermittence, and probability distribution. The implication of the measurements is discussed in section 5. In the Appendix, an

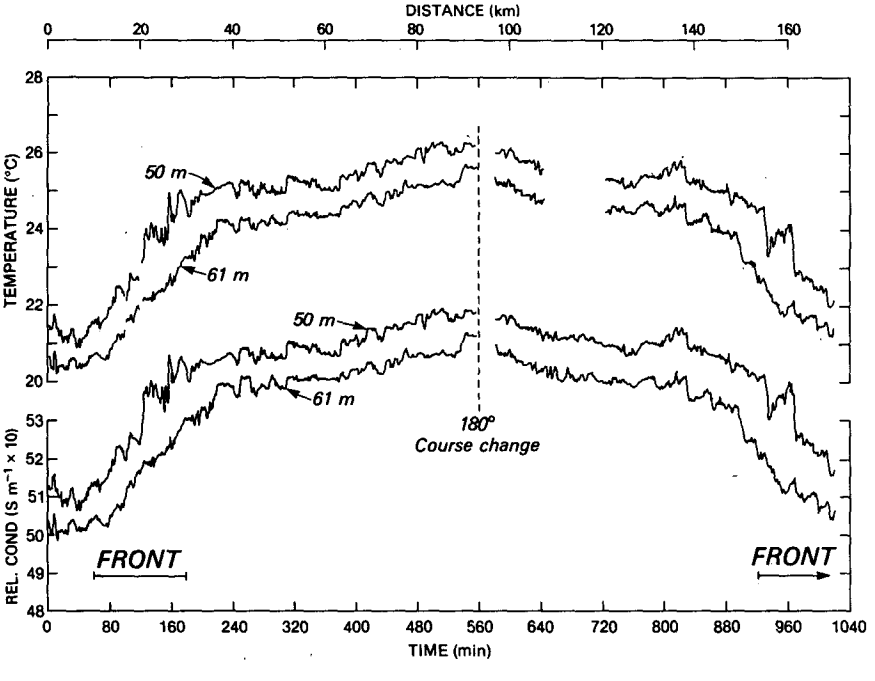

FIG. 1. One-minute averages of temperature and conductivity at the two depths of interest. Because of indeterminable offset changes in the calibration of the sensors, the conductivity scale is believed to be accurate in only a relative sense. Conductivity is measured in Siemens per m (S m^{-1}; 1 S m^{-1} = 10 mmho cm^{-1} ~ 10°C). A frontal zone indicated by the large horizontal gradient was intersected first in a tow to the north, then again in a southward tow. The 80 min periods correspond to individual data tapes. Data analyzed in the main body of the paper are from the 1020-min-long period beginning at 0 min, which corresponds to 0428 GMT 20 Jul 1981. The periods described in MRDS are 0–320 and 720–1040 min.

alternative method of processing is used to analyze some additional data and document the extent of the contamination problem.

2. Instrumentation

The conductivity sensors used in this study were dual-needle cells developed for the Naval Research Laboratory by the Applied Physics Laboratory of the University of Washington and described in Meagher et al. (1982). Each sensor consists of two 1.25-mm diameter forward-mounted platinized-platinum electrodes spaced 3 mm apart. Photographs of this sensor are shown in Dugan and Okawa (1982) and Okawa and Dugan (1984). Because of the two-electrode design, calibration stability is inferior to a four-electrode cell, such as the standard 3-cm rectangular Neil Brown Instrument Systems' cell. Meagher et al. (1982) measured calibration changes of $\pm 1.5 \times 10^{-3}$ S m^{-1} over periods of minutes to hours in the laboratory; unfortunately, much larger changes apparently occurred in the field (see Figs. 1 and 2). The spatial resolution of the needle cells, on the other hand, is quite good; the -3 dB point of the amplitude-squared response is about 0.7 cy cm^{-1} as determined by Meagher et al. (1982) by moving a prototype probe rapidly through an interface in a laboratory tank. In addition, Okawa and Dugan (1984) have studied the in situ response to small (<1 cm) particulates flowing through the sensing volume, and they found the -3 dB point to be about 440 Hz which translates to better than 1 cy cm^{-1} at the usual towing speeds (2.5 m s^{-1}). This latter estimate does not include the effects of the boundary layer on the sensor, so the spatial scale resolved by the system is assumed to be that determined by Meagher et al. (1982), i.e., a wavelength of about 1.5 cm.

The large dynamic range of the conductivity fluctuations is preserved by pre-emphasizing the high frequency part of the signal prior to recording. This technique substitutes for the usual method of separately recording high and low frequency signals. The pre-emphasis transfer function is

$$E_{\text{out}}/E_{\text{in}} \equiv H(\omega) = (1 + i\omega\tau_{12})/(1 + i\omega\tau_2), \quad (1)$$

where E_{in} and E_{out} are input and output voltages, $\omega = 2\pi f$, f being frequency in Hz; $\tau_{12} = (1/2\pi)(1/f_1 + 1/f_2)$, $\tau_2 = 1/2\pi f_2$; and, $f_1 = 0.25$ Hz and $f_2 = 200$ Hz. The function (1) has unity gain from DC to 0.25 Hz where it begins to rollup at 6 dB/octave (20 dB/decade); it then levels off near 200 Hz. [See Dugan and Okawa's (1982) Fig. 5.] For frequencies between 0.25 Hz and 200 Hz the data closely approximate a differentiated signal, i.e., for $\omega\tau_{12} \gg 1$ and $\omega\tau_2 \ll 1$, (1) reduces to $H(\omega) = i\omega(2/\pi)$; thus, $E_{\text{out}} = (2/\pi)\, dE_{\text{in}}/dt$. The conductivity, κ, equals E_{in} times the gain, G ($\sim$0.2 S m^{-1} v^{-1}); thus $d\kappa/dt = (\pi G/2) \times E_{\text{out}}$. For the data reported here the sampling rate was 500 Hz and an anti-aliasing filter was used that was set conservatively to be 3-dB down (in amplitude) at 170 Hz, rolling off at -48 dB/octave thereafter. The pre-emphasized data, then, are a combination of a mean conductivity signal (for $f \leqslant 0.25$ Hz) and a highpassed, differentiated signal (for 0.25 Hz $\leqslant f \leqslant$ 170 Hz). For a typical towing speed of $\sim$5 knots (2.6 m s^{-1}), the differentiated signal corre-

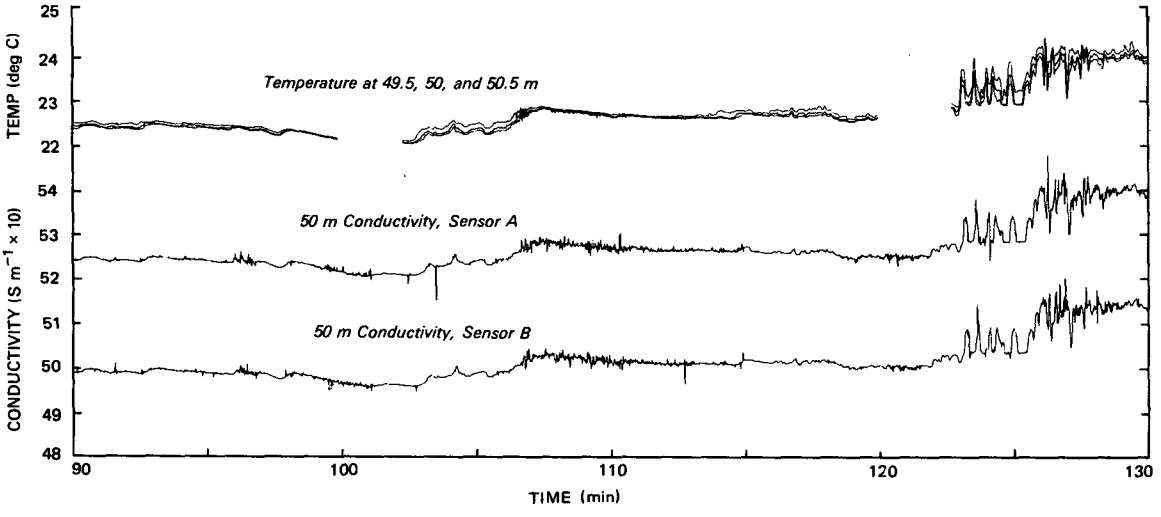

FIG. 2. One second averages at 50 m over a particular 40 min period. There are three temperature traces shown: The middle trace is from about the same depth as the conductivity series, the others are from 0.5 m shallower and deeper. The two conductivity series are offset from one another as a result of a change in the calibration of one or both of the sensors. Note that since part of the differentiated signal is included in a 1 s average, the conductivity series show evidence of microstructure events, e.g., at 100 and 110 min (cf. Fig. 7). Occasional spikes in the conductivity series are artifacts resulting from particulate spikes in the raw data. As described in the text, spikes are removed as part of the calculation of microstructure variance.

sponds to wavelengths less than several meters, and it will be mostly shorter scales that contribute most to the variance values to be shown later.

Signals from microstructure conductivity sensors in the open ocean suffer to some degree from contamination by organic (presumably, plankton) and inorganic particles in the water. The contamination is of two types: (1) discrete events, appearing in the data as "spikes" of ~3 ms duration, and (2) catastrophic fouling, which introduces long-term offsets and wideband noise into the data as a result of attachment of biological material within the cell volume. Examples of both types are shown in Okawa and Dugan (1984). As they point out, "the spikes are a crucial problem because they are so pervasive and because they can dominate the variance". (The occurrence of spikes in the present data is discussed in detail in the Appendix.) Although the dual-needle cell was developed to minimize the fouling, two complete and independent dual-needle systems were used at the same depth to further reduce the impact of a fouled cell. Later comparisons with other types of sensors have indeed indicated that it was better able to cope with biological matter in a noncatastrophic fashion (Meagher et al., 1982; Okawa and Dugan, 1984).

The conductivity electronics, including the pre-emphasis filter, were housed in a streamlined tow-body—a "fish"—and the two dual-needle cells were positioned at the ends of 15-cm-long horizontal arms. The fish was attached at a four-conductor breakout position on the towed thermistor chain (described by Morris et al., 1983). When under tow, the two conductivity sensors are pointed into the flow, about 30 cm apart in the cross-tow direction, and are behind (but not in the wake of) the towed chain.

The data in this paper are from two pairs of dual-needle cells: the upper (shallower) pair were on a fish located at breakout 105; the lower (deeper) pair on a fish at breakout 125. Over the course of the period analyzed, the corresponding mean depths (± one standard deviation) were 49.7 ± 2.0 m (for 105) and 60.8 ± 2.2 m (for 125), hereafter, 50 and 61 m. The tow-depth variations arise mostly as the chain adjusts to a changing vertical shear. For periods in the ship-motion band, vertical chain movement can be ignored as it is kept low (typical rms amplitude ± 2 cm) by use of a tensioner (Morris et al., 1983).

Thermistors were located at 75 cm intervals along the cable. At the depths of interest, this translates to vertical separations of 53 and 58 cm at 50 and 61 m, respectively. Exactly how close in depth the conductivity sensors were to the nearest thermistor once deployed is not known, but they are believed to have been within 10 cm (B. Okawa, personal communication, 1985). This is consistent with the generally excellent correlation between conductivity and nearby temperature. However, the lack of vertically colocated sensors has precluded the routine calculation of salinity changes over the small horizontal scales of most interest here. One second averages of temperature are used in this work and these have a relative accuracy of 0.01°C.

3. Analysis methods

The conductivity data chosen for analysis are from the period 0428–2128 GMT, 0 to 1020 min in Fig. 1. Data earlier than this had several problems (a fouled sensor, lack of concurrent temperature data, time gaps) which made their analysis incompatible with the scheme described below. However, some of these earlier data will be presented in the Appendix.

a. Conductivity versus temperature

Salinity variations in the study area were generally small (e.g., Trump et al., 1985). A typical profile had a weak maximum in the depth range 30–50 m below which a decrease of ~0.1 ppt per 100 m was found. As a result, temperature changes dominate the conductivity signals on the finescale (e.g., Fig. 1 and 2). It will be assumed that this behavior extends to the smallest scales resolved, allowing the temperature variance to be estimated from the conductivity signal. As the conversion factor between conductivity and temperature is nearly unity, we will use a constant value of $1°C/(0.1\ S\ m^{-1})$ for $\partial T/\partial \kappa$. Also, for simplicity, values of microstructure (conductivity) gradient variance will be expressed in temperature units.

b. Calculation of microstructure variance

An initial problem was to eliminate the particulate spikes which, since they occur irregularly in the data, can give rise to spurious spatial variability in the variance. This contamination problem was alleviated by taking advantage of the redundancy provided by the two sensors on each fish. Since patches tend to be of a width large compared with the sensor spacing, each sensor provides an independent sample of the turbulence in a patch. [For example, note the simultaneous patches in the conductivity traces in Fig. 2, or in Okawa and Dugan's (1984) Fig. 3, their curves 2A and 2B being our 50 m sensors, and their 3A and 3B our 61 m sensors.] On the other hand, the spikes occur on each sensor independently and this is used to remove their effect on the variance as described below.

At each depth, variances were calculated for both sensors over contiguous data segments each of a length less than the expected interval between spikes, but only the *minimum* variance was retained for each segment. According to Okawa and Dugan, the mode and mean of the time interval between spike encounters was 0.18 and 0.43 s, respectively. (They examined only 80 min of data, but their conclusions are consistent with the analysis in the Appendix.) Therefore, it would be highly unlikely to observe consecutive spikes within a time interval shorter than about 100 ms, so the segment length was chosen to be 50 ms (25 data values long).

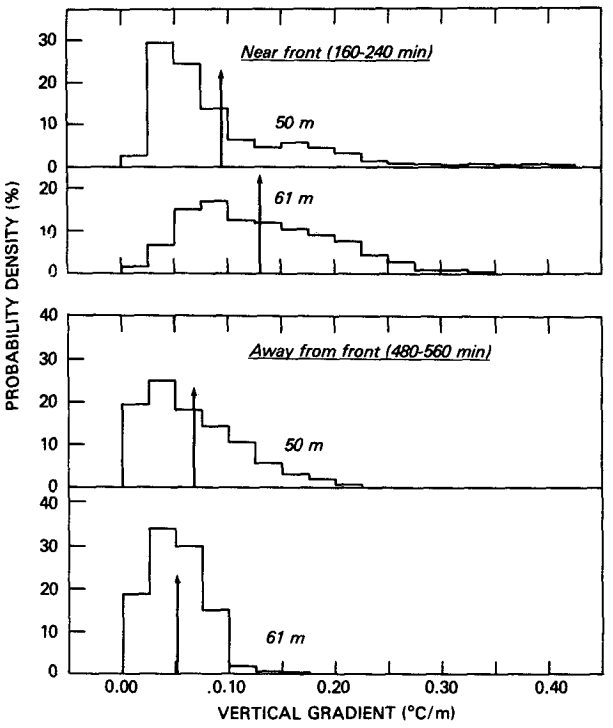

FIG. 3. Histograms of $\partial T/\partial z$, shown for two 80-min periods. $\partial T/\partial z$ is calculated as $\Delta T/\Delta z$, where ΔT is a centered difference averaged over 1 s and Δz is the vertical separation, about 1 m. The vertical arrows show the mean values. The distributions are not Gaussian, but skewed, with a most probable value (mode) as small as one half the mean and a tail extending to large gradients. These distributions are similar to ones exhibited by Hayes et al. (1975), Gregg and Sanford (1980), and Desaubies and Gregg (1981) for vertical separations less than about 2 m.

Processing with a different segment length (100 ms, say) would be expected to give nearly identical results and, indeed, this was found to be the case.

As part of the computation, certain other "noise" was eliminated as well. This noise also took the form of discrete events or spikes, but occurred simultaneously in all recorded conductivity channels, and is presumed to have been caused by a system problem. The problem occurred irregularly and most often early in the dataset, producing ~10 spikes per 80 min tape. Although the largest could have been simply edited out, a spike-detecting algorithm was used to systematically eliminate them from the data. The algorithm worked by detecting any minimum variance value that exceeded a 1 s mean variance by at least 11 standard deviations and replacing such anomalous variances with a corrected 1 s mean. (See the Appendix for discussion of a similar algorithm.) The 11 s.d. criterion was very stringent, designed to eliminate only spurious values.

One-second values of the minimum variance were obtained by averaging over twenty 50-ms segments. These were converted to conductivity gradient variance, $\langle(d\kappa/dx)^2\rangle$, by multiplying by U^{-2}, U being the average ship's speed relative to the water at the depth of the sensors. A constant value of 280 cm s^{-1} was used for U (C. Trump, personal communication, 1984). Fluctuations in U were less than 25 cm s^{-1}, resulting in a relative error in the variance of less than 20 percent. Our estimate of the microstructure temperature gradient variance (hereafter, simply variance) is, then, $\langle(dT/dx)^2\rangle = \langle(d\kappa/dx)^2\rangle\langle(\partial T/\partial\kappa)^2$.

While the preceding approach was fairly easy to implement and allows for the efficient processing of a large amount of data, retaining only the minimum variance clearly biases the results on the low side. Whether inside or outside a patch, natural spatial variability can cause signal levels at the two sensors to be significantly different (e.g., Fig. 9). As an estimate of this effect in the case of an energetic patch, the variance contribution from each sensor was computed separately. Spikes as well as real signal were necessarily included in this calculation, but the evidence is that the spikes account for, at most, 1% of the variance in such a patch (see Appendix). The result in this case was that the minimum variance accounts for only 59% and 60% of the individual sensor variances, so the bias is significant. Similar underestimation can probably be expected in other patches; thus, a systematic error is present in the analysis. (An independent treatment of the data, presented in the Appendix, analyzes data from only one sensor at a time, eliminating this bias. Qualitatively, the results are quite similar.)

A more significant problem is the limited bandwidth of the measurements, resulting in the variance again being underestimated. The magnitude of this effect is indeterminable, but the variance-preserving spectra of Gargett (1978), Dillon and Caldwell (1980), and Washburn and Gibson (1982) suggest the error could be as large as a factor of two. Since the most energetic patches will be seen to account for a large fraction of the total variance, the underestimation is not negligible. Added to the minimum-variance bias, some variance values may, then, be low by a factor of about 4. These errors are not believed to affect the main results in a significant way.

c. *Computing Cox numbers*

The Cox number is defined as (e.g., Caldwell, 1983)

$$C = \langle(\nabla T)^2\rangle/\langle\partial T/\partial z\rangle^2. \quad (2)$$

In order to estimate the Cox number from the one-dimensional towed data, some assumption must be made about the missing components of the gradient. We assume isotropy, so that, in (2), $\langle(\nabla T)^2\rangle$ is replaced by $3\langle(\partial T/\partial x)^2\rangle$. Values of $\langle\partial T/\partial z\rangle$ were calculated as $\Delta T/\Delta z$, where ΔT is the vertical difference centered at the depth of a microstructure sensor and $\Delta z \sim 1$ m is the corresponding depth difference. Values of ΔT were calculated as 1 s averages and, so, $\langle\partial T/\partial z\rangle$ represents

about a 1 m vertical by 2.8 m hortizontal estimate. For values of $\Delta T < 0.01$°C, a value of 0.01°C was used. As defined in (2), $C = 0$ (not $C = 1$) corresponds to the case of laminar motion, i.e., no turbulent heat transport. For low values of C, the assumption of isotropy breaks down and the approximation used for $\langle(\nabla T)^2\rangle$ is no longer justifiable. Furthermore, in our usage $\partial T/\partial x$ may contain contributions from relatively low-wavenumber fluctuations that do not go to zero for the case of laminar flow. For these reasons, the physical interpretation of low values of C is not straightforward; however, since the main interest is in large Cox number events, this is not a severe limitation.

Errors in the Cox number calculation include those for the variance plus errors in the estimation of $\langle\partial T/\partial z\rangle$. In general, for the Cox number to be meaningful, the mean gradient must be representative of the stratification upon which the fluctuating motion is acting (Caldwell, 1983; Dillon, 1982, 1984). Dillon typically calculates the mean gradient in a manner essentially equivalent to dividing the maximum temperature difference within an event by the event height, which he finds to be <1 m in the seasonal thermocline (see Tables 1 and 2 in Dillon, 1982). The use of a fixed vertical interval in the present work is clearly a shortcoming, since it is only the case where an event just fills the 1 m space between the thermistors that the estimates of $\langle\partial T/\partial z\rangle$ are correct in Dillon's sense, although even then they remain limited by the thermistor intercalibration error. There is some evidence that the probability density function of the vertical temperature difference does not change appreciably for difference intervals in the range 0.1 to 1.0 m (Desaubies and Gregg, 1981); therefore, for an event thinner than 1 m, we may be as likely underestimating as overestimating $\langle\partial T/\partial z\rangle$. For an event much thicker than 1 m, underestimation is, perhaps, more likely as the average gradient where the fluid is mixing ought to be less than that inferred from the ambient fluid just outside the event boundaries. We conjecture that, on the average, the errors may not be severe.

The use of long-term averages of the mean gradient as done by Washburn and Gibson (1984) is much more likely to produce erroneous values of Cox number. There is simply too much variability in the vertical gradient to expect that kind of average to be representative of the gradient at the time of the fluctuations. In our work, for example, $\langle\partial T/\partial z\rangle$ varies at a given depth by an order of magnitude over an 80 min long tow section (Fig. 3); as a result, the Cox number can vary by a factor of 100 solely because of a changing background stratification. It is important to note that negative values of $\langle\partial T/\partial z\rangle$ are rare, none being found in the Fig. 3 periods, for example. Temperature inversions do occur in the data, especially near the front where they are likely the result of intrusions, but these are not so substantial near 50 and 61 m as they are shallower. In the entire 61 m record, only one occurrence of an inversion (a value of -0.01°C m^{-1}) was found and this was associated with an extensive event (see Fig. 7).

4. Results

a. *Large-scale variability*

Time series of microstructure variance and Cox number over the entire dataset are shown in Fig. 4. The signal intensities vary over many decades, generally in unison, but the relative significance of individual variance events varies considerably, depending upon the magnitude of the local temperature gradient. The corresponding cumulative distributions (Fig. 5) are clearly made nonuniform by a few large events in the frontal zone that account for a large fraction of the total mixing. Average variance values, obtained by dividing the total sums by the record length, are 1.3 $\times 10^{-6}$ and 1.0 $\times 10^{-6}$ (°C cm^{-1})^2 at 50 and 61 m, respectively; average Cox numbers are 3 and 18. These are to be considered lower bounds, of course, since the variances are under-resolved as discussed in section 3. Variance records for the period prior to that in Fig. 4, which come from the southernmost part of the survey

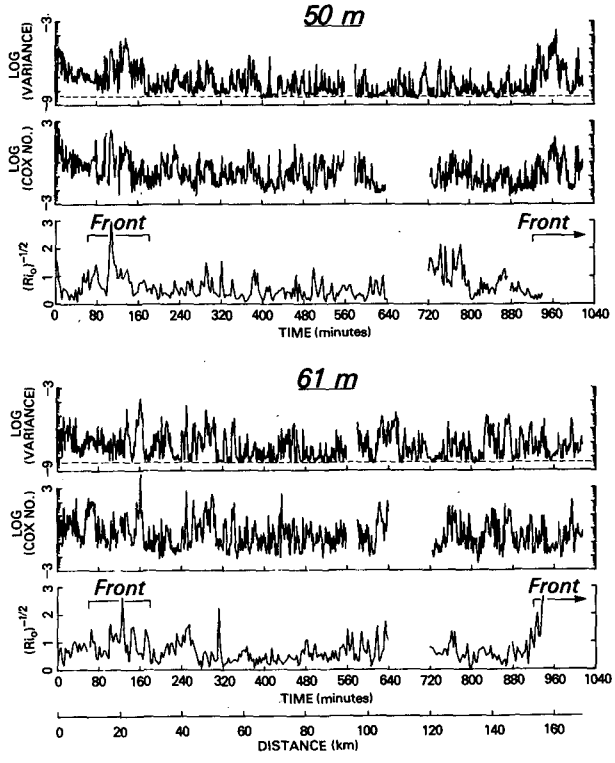

FIG. 4. Time series of microstructure variance, in units of (°C cm^{-1})^2, and Cox number (both 1 min averages), and $(Ri_0)^{-1/2}$ (3 min average). Ri_0 is a large-scale Richardson number; plotting its inverse square root accentuates the low Richardson number events. The approximate value of the variance noise is indicated by the horizontal dashed line.

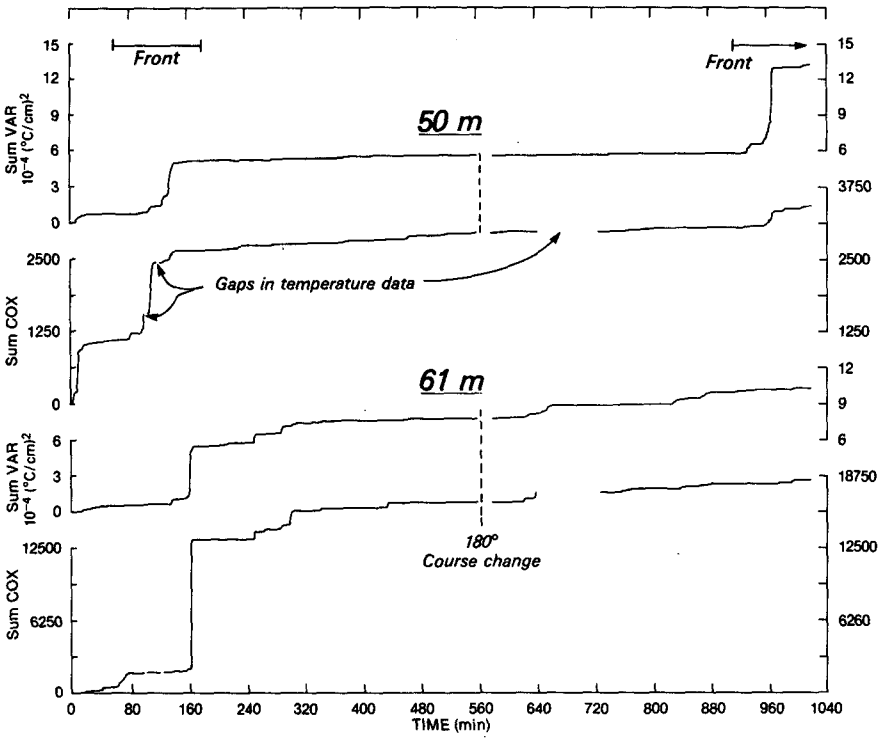

FIG. 5. Cumulative distributions of variance and Cox number at 50 m (top two curves) and 61 m (bottom curves).

area, are shown in the Appendix (Fig. A1). At 50 m, levels lie below 10^{-5} (°C cm^{-1})^2, less than in the two frontal events at that depth, but greater than the levels north of the front; at 61 m, levels exceed 10^{-5} (°C cm^{-1})^2 in several places. Indeed, there is some evidence (Mied et al., unpublished manuscript) that the southern area was dynamically more active than the area to the north.

Velocity measurements made with an acoustic Doppler system (Trump et al., 1985) have been merged with the temperatures to provide values of a large-scale Richardson number, Ri_0. Occurrences of low values of Ri_0 are believed to serve as, at least, a qualitative indicator of the fluid's propensity to develop instabilities that lead to mixing (cf. D'Asaro, 1985). The Ri_0 was calculated as $\langle N^2\rangle/\langle S\rangle^2$, where the brackets denote 3 min (~450 m) horizontal averages, and $\langle N^2\rangle$ was calculated from the temperature field only as $\alpha g\langle \Delta T\rangle/\Delta z$, where α is the expansion coefficient and g is the gravitational acceleration. Vertical centered differences over 1 m were used after both the velocity and temperature fields were smoothed and interpolated to a common vertical 0.5 m grid (C. Shen, personal communication, 1984). This is somewhat different from the procedure used in MRDS, but the results (Fig. 4) are similar. Overall there is no trend between the occurrence of high Cox number events and large values of $(\mathrm{Ri}_0)^{-1/2}$. MRDS show only a suggestion of a relationship between low values of Ri_0 and the finestructure level in the limited region of the front. As a predictor of the precise location of mixing events, the large-scale Richardson number used here appears, then, to have little value. Recent work (e.g., Padman and Jones, 1985) suggests that the probability of occurrence of critically low values of a small-scale Richardson number is very sensitive to not only the background state (of which Ri_0 may be an adequate measure), but to the variance of the shear and density gradient. It is possible, for example, that a more detailed examination of the shear variance from the Doppler data may be useful, but this has not been done.

The horizontal scale of microstructure events is of interest because it may be an indicator of particular classes of mixing processes. However, defining an event width from a single one-dimensional slice through an event is often made difficult by high levels of intermittency (cf. Atlas et al., 1970). Nevertheless, an attempt was made to quantify the widths by measuring the distance between successive up-crossings and down-crossings of a chosen threshold level. The variance series were used for the detection process since a constant threshold could most easily be defined in that case; however, similar widths are expected to hold for the Cox number series. From inspection of the original data and many plots of 1 s data, it is clear that many patches are on the order of tens of meters wide. These

are not treated in the present analysis which uses the 1 min (~170 m) averages, but their dominance will be clear from the trend in the results. The threshold level was set at 4×10^{-8} (°C cm^{-1})^2, a decade above the mean noise level (~4×10^{-9} (°C cm^{-1})^2, as judged from examination of the quietest records). This excludes from the results both the fluctuations associated with very low signals and those associated with real variability in the elevated signal within the stronger events. The results (Fig. 6) show similar distributions at both depths. As defined, most events are less than 1 km wide; very wide events do occur but are rare. Over the limited range of width values calculated, the results can be fit according to (number of events) $\propto$ (event width)$^{-D}$, if D is about 1.6. In discussions of scaling laws in turbulence, D is regarded as the fractal dimension (e.g., Schertzer and Lovejoy, 1984).

b. *Detailed view of the largest events*

Detailed time series of variance are shown in Fig. 7 for periods including the most significant events at each depth. The Cox numbers (not shown) can be inferred from the variance time series by taking into account the changing temperature gradient, which can be estimated from the two temperature traces shown. For a constant gradient, the Cox number is linearly proportional to the variance, so that in a scatter plot of log$C$ against log variance, successive points will fall along lines of unit slope. An example is shown in Fig. 8 for the data at 61 m. Deviations occur for a variable $\partial T/\partial z$ so that, for a fixed variance, points are constrained to fall between two bounding lines of constant $\partial T/\partial z$: the upper line corresponding to $\partial T/\partial z = 0.01$°C m^{-1}, which results from our having chosen $\Delta T_{\min} = 0.01$°C as the smallest resolvable value; the lower line corresponding to the largest observed $\partial T/\partial z$ which, in the case of Fig. 8, is about 0.3°C m^{-1}. Notice that very few points fall near the upper line, suggesting the Cox number calculations are not overly constrained by the least count value of $\partial T/\partial z$.

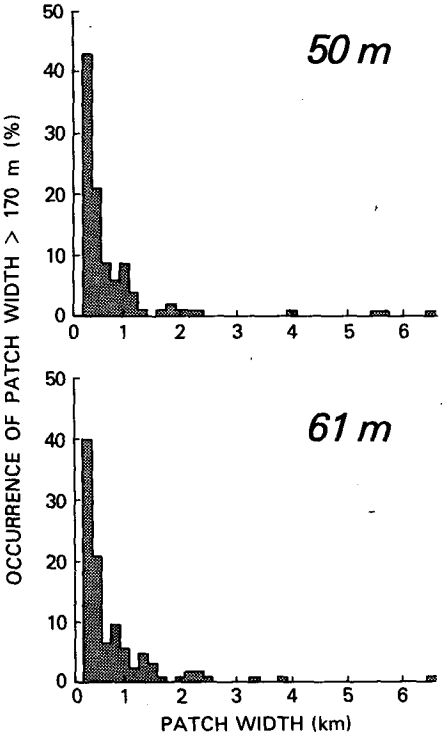

FIG. 6. Histogram of patch widths based on the data of Fig. 4. See text for details.

The variance levels along either depth are clearly highly intermittent. Many events begin and end very abruptly, as if the sensor had suddenly passed through a boundary separating non-turbulent from turbulent fluid. Some of this *external* intermittency seems to be associated with internal waves, e.g., near the end of the 50 m series in Fig. 7, or, at other times, with a glancing encounter with a nearby event, e.g., at about 91.5 min in the 50 m series. Because of our concern over spurious spikes in the data (from either particulate matter or electronic noise), this latter event, which, because of its extremely narrow width does look suspicious, was examined in detail by computing the deemphasized (i.e., undifferentiated series) for both sensors. The results (Fig. 9) show an event of about 1 s (~2.8 m) duration, which looks different in detail at each sensor but shows the same qualitative characteristics. Not only are there large fluctuations during the event, but the mean temperature increases as well, as if a completely different piece of water, presumably lying mostly above 50 m, was sampled. We conclude that the event contains real microstructure. After this first event, the signals continue to be quite similar for several seconds (~10 m) until sensor B detects a very narrow event, again warmer than the surrounding fluid along the sampling path. The ~60 ms (~18 cm) width of this event is greater than that expected for a spurious spike, so we are led to believe it is real as well; however, since this event occurs only at sensor B it is eliminated by the minimum variance calculation and, thus, does not appear in the Fig. 7 series.

In order to better interpret the variability in the towed microstructure data, the simultaneous two-dimensional temperature finestructure data of MRDS is also shown in Fig. 7. Briefly, each little square shown represents a temperature variance calculated as a 16 s (~42 m) average for the horizontal wavelength band of 1–3 m and normalized by the square of the 16 s average vertical temperature difference. The normalization removes unwanted modulation of the variance levels by changes in the magnitude of the background vertical stratification. For purposes of display, only values in excess of some cutoff value (10^{-4} in the present case) are shown. For every step increase in the intensity of the grey scale, the normalized variance in-

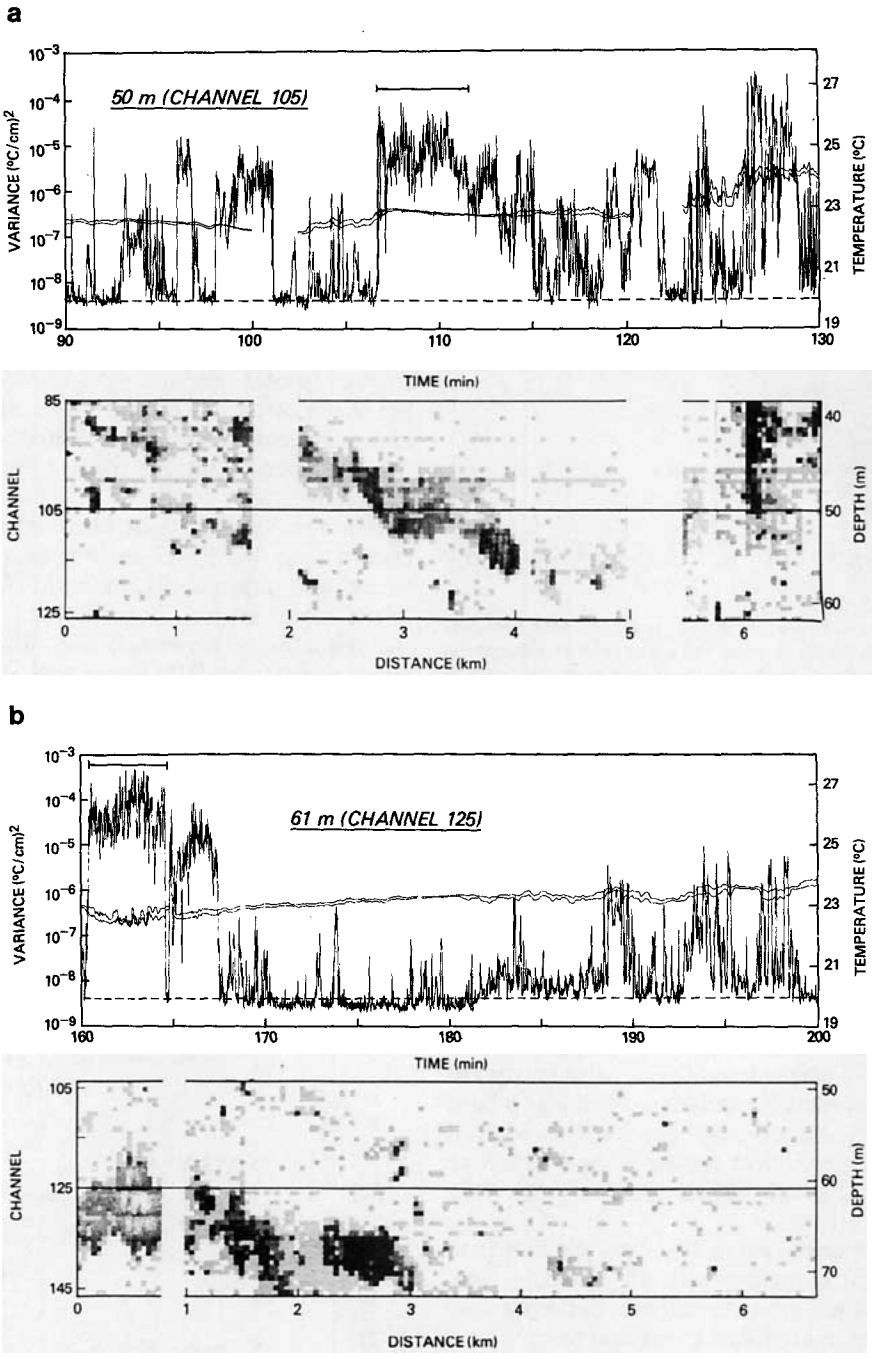

FIG. 7. Microstructure records for the two largest mixing events compared with sections of finestructure patches (modified from Rosenblum et al., 1985). The temperature records shown in the upper panels were obtained from sensors 0.5 m above and below the microstructure probe and are the ones used to estimate $\langle \partial T/\partial z \rangle$ in the Cox number calculations. The horizontal bars show the segments of microstructure data used to compute the histograms in Fig. 10. The normalized finestructure variance (lower panels) increases logarithmically according to the intensity of the grey scale. White corresponds to values less than 10^{-4}; the darkest shading (which, in the figure, is not reproduced with uniform consistency) is about 10^{-1}. See text for details.

creases by half a decade. The finestructure variability is such that the higher signal levels appear only in areas of finite extent or, hereafter, "patches." The microstructure data can now be further analyzed with due regard to the path of the probes through this two-dimensional patch field.

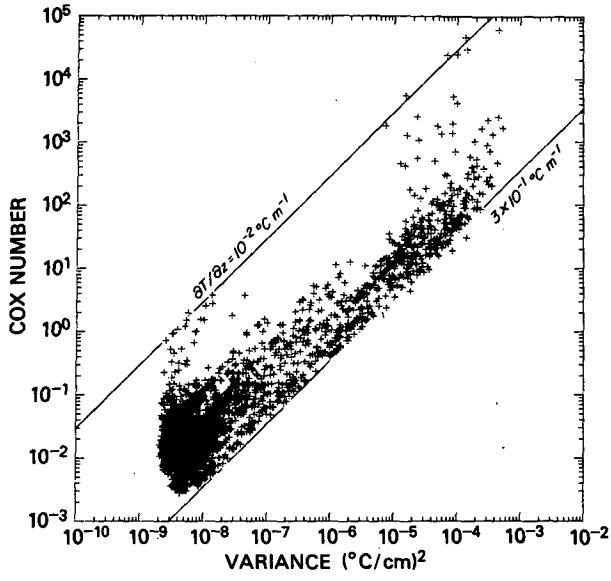

FIG. 8. Scatter plot of Cox number against variance at 61 m, corresponding in time to the Fig. 7 series. For a given variance the points are constrained to lie between the two lines shown, as discussed in the text.

In the 50 m case, it can rather neatly be seen that the large microstructure event at around 110 min represents a slice through an approximately 5 m high finestructure patch that is horizontally coherent over several kilometers but is deepening with increasing distance along the tow. The microstructure event begins abruptly apparently because the corresponding finestructure patch does so, and it ends more gradually as the patch gradually moves deeper than the measurement plane. The *internal* intermittency of the microstructure event also seems reflected in the patch. Many of the other large-amplitude events can also be seen to coincide with finestructure patches, most of which have significant vertical extent. Also, the narrow event at 91.5 min does, indeed, now appear to be a sampling of the bottom of a small, but relatively intense, finestructure patch.

In the 61 m records, before 170 min, the large microstructure event coincides with an extensive finestructure patch which subsequently moves deeper than 61 m. At 189 min, a moderate event and patch occur. Finally, intermittent events occur in the presence of internal waves at the end of the record, possibly indicating a vertical wafting of a single-sensor patch (along channel 126) into and out of the path of the microstructure probe. It is important to note that a detailed examination shows many lower-amplitude events do not have corresponding patches. This is clearest in the 61 m record which has only a few conspicuous patches.

c. *The question of log-normality*

In fully turbulent flows the variance of many gradient quantities (e.g., dissipation) has a lognormal or nearly lognormal distribution as the result of the intermittency of the cascade of variance to smaller scales. Lognormal distributions are found in ocean microstructure data as well, but these are believed to result from finestructure modulation and the intermittency associated with sampling different events, as well as the statistical variability within an individual event; thus, these distributions are not evidence for "universal" oceanic turbulence (Gregg, 1980). However, it may be possible to carefully isolate a small part of a microstructure event and find that the distribution of the variance or Cox number is approximately lognormal; on the other hand, without careful selection for possible turbulent events, the shape of the distribution over an extensive set of data will depend upon the degree of modulation by the finestructure and the relative proportion of events to non-events.

In order to explore these ideas, segments of data were chosen from the Fig. 7 records to represent the most active (and, presumably, the most turbulentlike) parts of the major events. These segments are indicated in the figure by the horizontal bars, which begin and end where signal levels fall off abruptly. Histograms of these data are shown in Figs. 10a and 10c. For comparison, calculations have also been done for the entire Fig. 7 periods (Figs. 10b and 10d).

The limited, energetic segments of the events do, indeed, have variance distributions that are (by eye) approximately lognormal. At 50 m the mean is 6.2 $\times 10^{-6}$ $(°C\ cm^{-1})^2$. The distribution of Cox numbers is also roughly lognormal; the average is 102, with values larger than 10^3 being found. At 61 m the variance distribution is also approximately lognormal, but the Cox number distribution appears to be positively

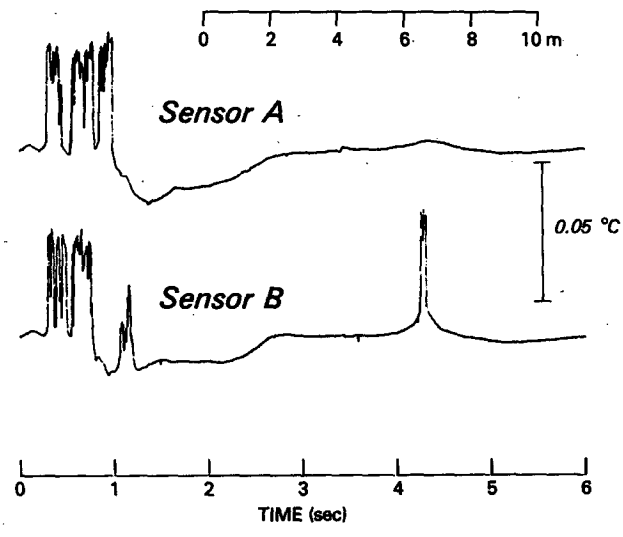

FIG. 9. De-emphasized microstructure time series corresponding to the isolated event at about 91.5 min in the 50 m record of Fig. 7. The sensors were spaced 30 cm apart in the horizontal. The event at $t = 4$ s is about 0.06 s (18 cm) wide.

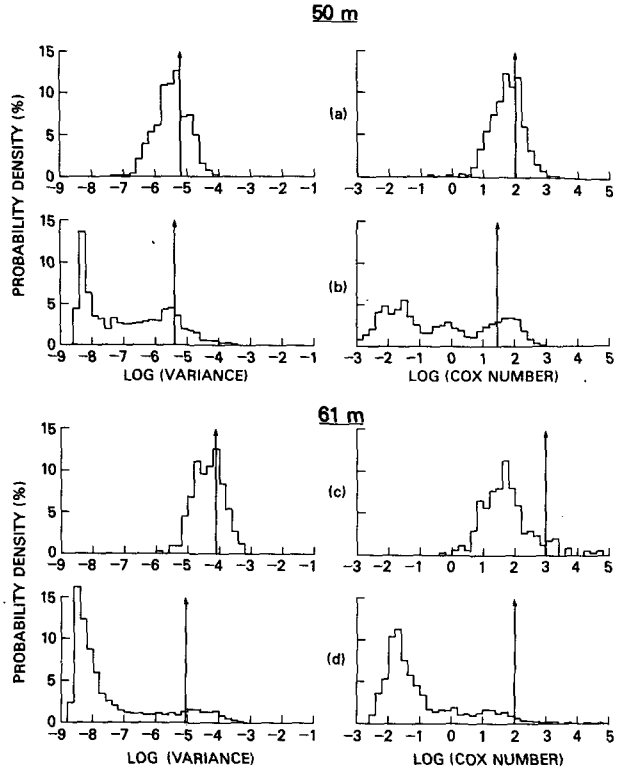

FIG. 10. Histograms of variance and Cox number. Results for the two largest events alone are shown in (a) for the patch at 50 m (for 380 values) and in (c) for the 61 m patch (250 values) as indicated in Fig. 7. The results in (b) and (d) cover the entire periods shown in Fig. 7 (2400 values). The vertical arrows show locations of the mean values.

skewed from a single lognormal fit as a result of an excess of values lying a decade and more beyond the mean. The mean variance is 7.6×10^{-5} $(°C\ cm^{-1})^2$ and the mean Cox number is 950, both about 10 times the 50 m values.

When data outside the most energetic events are included, the distributions become much wider (Figs. 10b and 10d) as other events have filled in the available multidecade-long space between the noise level (4×10^{-9}) and the high energy end. The rise in the distribution as variance levels decrease towards 10^{-8} is believed to be real, suggesting that, in the absence of noise, this part of the distribution would shift to still lower values; as shown, the modes are about three decades below the means. An important point is that each distribution includes more than 6 km of data (about the amount Washburn and Gibson, 1984, examined), yet there would be considerable ambiguity in fitting them with a single lognormal curve.

The rate of dissipation of temperature variance, χ, is equal to twice the thermal diffusivity times $(\nabla T)^2$. For these data, χ estimates range from a noise-contaminated mode of $\sim 3 \times 10^{-11}$ to nearly 10^{-5} $°C^2\ s^{-1}$ in the most energetic events. For comparison, in the main thermocline, Gregg (1980) found χ values of 10^{-12}–10^{-7} $°C^2\ s^{-1}$, and the mode for the MILE thermocline was estimated by Washburn and Gibson to be $\sim 4 \times 10^{-10}$ $°C^2\ s^{-1}$.

5. Discussion

a. *Event characterization*

The characterization of the extreme variability of microstructure levels is dependent upon sensor noise level. The view obtained by Washburn and Gibson (1984) is one of very narrow events (average width ~ 7 m) occurring in "clouds" or "clusters" of much larger extent (~ hundreds of meters), but this characterization may be biased by their rather high noise level of $\sim 2.9 \times 10^{-5}$ $(°C\ cm^{-1})^2$. As an example of the potential for bias, imagine the Fig. 7 results with the noise floor moved up to 3×10^{-5}, say. The events that are resolved do, indeed, resemble occasional clusters of very narrow, seemingly separate events. When the noise level is lowered, former clusters may alternately be viewed as spatially coherent events with internally intermittent structure. Of course, in our data, too, a clear characterization becomes impossible for those events having signal levels approaching the noise floor.

The scale of the external intermittency of the observed microstructure events can be at least partly understood by comparisons with the finescale variability (e.g., Fig. 7). The small-scale internal intermittency is presumed to result from the detailed dynamics occurring within a particular event, and the scale of that variability can be quite small indeed. Variations over scales $\leqslant 10$ m are not uncommon, and this scale size is similar to Washburn and Gibson's result. This internal variability is, perhaps, consistent with the general observation from vertical profile measurements that quite often a single microstructure patch is composed of a number of smaller overturning eddies (e.g., Caldwell, 1983).

b. *Mixing processes*

What is responsible for the small-scale activity? The spatially persistent connection between many of the microstructure events and finestructure patches (e.g., Fig. 7) certainly suggests a physical connection between the two. MRDS suggest that the extensive patches are maintained by overturning internal waves; the microstructure then results from the ensuing smaller scale straining motion. Whether this can actually be *demonstrated* by a detailed comparison between the microscale fluctuations and the larger scale structures within the patch will be the subject of a future paper. The large-amplitude events likely dominate the microstructure–finestructure correlation values calculated by MRDS, and this accounts for the nonuniformity in the mixing parameters (e.g., Fig. 5). However, there seems to be an underlying uniformity present, as well, which

should not be ignored. This appears in Fig. 5 as a more-or-less continuous increase in the cumulative signal; and Figs. 4, 7, and A1 show that the microstructure levels are rarely without some resolved activity, suggesting that mixing at some level at least is occurring rather uniformly throughout the thermocline.

The relationship of the microstructure to changes in the stratification has not been sufficiently examined. We have been conservative in the treatment of conductivity data because of the fouling issue and their physical separation from the temperature measurements, and have not been confident in using them to calculate salinity. As a result, quasi-horizontal values of $R_\rho = \alpha\Delta T/\beta\Delta S$ could not be routinely computed and compared with the likelihood of occurrence of an event. Low values of $R\rho$ would indicate favorable conditions for salt fingering. Gargett and Schmitt (1982) found strong evidence for salt fingering in towed data at several depths where $R\rho$ (calculated on the basis of the average profiles) was less than 3 or so, but none where $R\rho$ was about 8. In our case, CTD (conductivity–temperature–depth) measurements made soon after the towing operations ended show (C. Trump, personal communication, 1984) that $R\rho \sim 10$ based on the general shapes of the profiles at the depths of interest, but that over limited depth intervals ($\sim$10 m thick) $R\rho$ approached values of 3 or 4; thus, we cannot rule out the intermittent occurrence of salt fingers in our data, and their importance may be all the greater away from areas of persistent shear. In fact, some segments of data well away from the front do seem to have the limited-amplitude, limited-bandwidth characteristics cited by Gargett and Schmitt, but whether this alone can be shown to provide sufficient evidence for salt fingering requires much more detailed study.

c. *Sampling considerations*

Under the presumption that the MRDS finestructure patches suitably flag significant mixing events, one must consider the view that the energetic events in the frontal zone were, more or less, sampled by chance and would have been missed had the probes been displaced a few meters vertically. For example, the 61 m record contains a very large event for the first frontal crossing, but a similar event was not found when the front was recrossed because the significant patches occurred at depths not sampled by the microstructure probe. It is not difficult, for example, to choose a sampling depth such that every significant patch shown in MRDS is missed or to choose another path that samples only patches outside the front, thus, giving a very misleading view of where mixing is occurring.

Given the preponderance of large patches near the front, these paths might not be the most likely ones, but they are possible, nonetheless. We conclude that a limited number of tows with only a few microstructure sensors cannot generally be relied upon to provide statistically valid estimates of the *number* of high energy events. Also, the observed signal *levels,* which in our case are not quantitatively reliable to begin with, must be viewed with the intermittency in mind. As Dillon and Caldwell (1980) point out, caution should be used in attempting to obtain volume averages of mixing parameters in the thermocline. This all supports Gibson's (1982) warning that the microstructure distribution might not be well determined even in the face of a considerable amount of sampling.

Acknowledgments. The high quality of the conductivity data is a result of the meticulous care and engineering skill of Benn Okawa and Tom Meagher. Bill Morris supervised the collection and processing of the thermistor data. The Richardson number results derive from Colin Shen's careful merging of the thermistor chain data with Clifford Trump's analysis of the Doppler data. Ms. Carol Pasquini typed the manuscript. This is a contribution to NRL's Finescale and Microscale Variability Program.

APPENDIX

Alternative Processing Scheme

The processing scheme described in section 3 relies upon redundant sensors to eliminate spurious signals caused by encounters with particulate matter in the water. Here, an alternate method is described and used to process additional data from south of the front which could not be previously treated. The results have been discussed in section 4. As a by-product, information is obtained about the spatial distribution of the particulate spikes. The spikes represent a contamination problem not only for conductivity probes but for hot or cold film sensors as well (e.g., Gargett, 1978, Fig. 2); and Nasmyth (1980) alludes to the problem of plankton concentrations sometimes being so high that data from turbulence sensors cannot be meaningfully interpreted. Previously, Okawa and Dugan (1984) have used a time-domain matched filter to detect and count the spike waveforms over an 80-min-long section; however, they make no mention of how general their results may be. Since the raw data show considerable spatial variability, the question arises as to whether there may be an increase in the spike density near the front, or a depth dependency, that would interfere with measuring the turbulent signal.

The detection algorithm used here works on a single data series as follows. Each second of data is divided into N segments (20 were used, giving 25 data points in each segment) and a variance, V_i, calculated for each. The mean variance, $\langle V \rangle$, and the standard deviation, σ_v, are calculated after excluding the three largest V_i. A "spike" is then detected in the ith segment ($i = 1, \cdots, 20$) if $V_i - \langle V \rangle$ exceeds a threshold level of $m\sigma_v$. A final 1 s mean variance is then calculated using only

the acceptable segments. Large values of m are used to avoid removing valid microstructure data. By Chebyshev's Inequality, $Pr\{|V - \langle V\rangle| > m\sigma_v\} < 1/m^2$, so, for large m, there is a low probability of detecting spikes. A value of σ_v must, therefore, be obtained that is minimally contaminated by the spikes; this, then, is the reason behind the prior removal of the three largest values. The three values are only candidates for spikes, however, and, after σ_v is calculated, must be examined as described above. In fact, the maximum number of three spikes per second is encountered very rarely, so the value three is a reasonable choice. (Where three per second are found we may, of course, be underresolving the number of spikes.)

Spike counts and variance for a detection threshold of $7\sigma_v$ are shown in Fig. A1. A close examination shows the spike counts to be highest when the variance is low (and detectability most likely) and least when the variance is high; but nowhere are spike numbers sustained at the maximum allowable rate of 180 min^{-1} (3 per sec times 60); thus, it is the microstructure variability that masks the true variability of the spike density, and not the other way around. Maximum spike numbers may increase near the front (cf. the two large variance events at 50 m which occur in the front), but the effect is not large. Likewise, the evidence for an increase at night (as a result of upward migration of zooplankton?) is not strong. There is no clear depth dependence, either. The number of spikes detected is, of course, a function of the detection threshold and there is a substantial increase as the threshold is lowered as shown in Fig. A2.

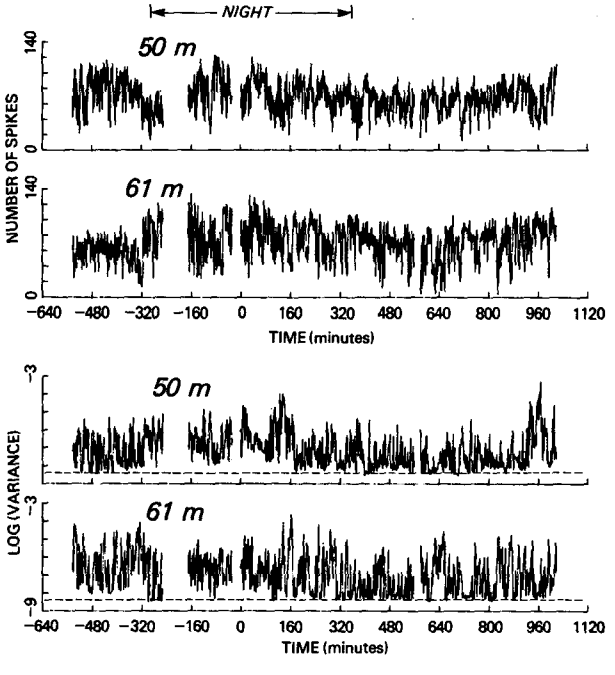

FIG. A1. Spike counts and variance (1 min averages) for a threshold level of 7 standard deviations. The period examined in the main body of the paper begins at a time of zero minutes. The true spatial variability of spikes is difficult to judge because of the masking effect of the microstructure, but if attention is paid to only the large-scale trend of the maximum numbers observed, there may be some slight association with either the front or with time of day. For reference, 120 spikes min^{-1} means one spike about every 1.5 m.

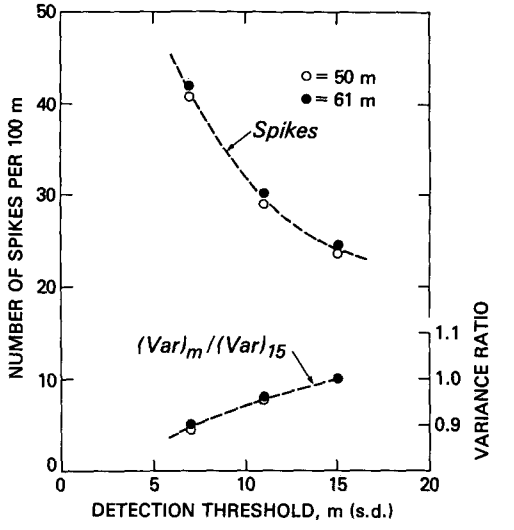

FIG. A2. Dependence of spike count (in numbers per 100 m of horizontal tow) and variance upon the detection level, m (in standard deviations, s.d., above the mean). Results for m = 7, 11 and 15 are shown. Variance results at m = 7 and 11 are shown relative to the m = 15 values.

The dependence of the variance upon the detection threshold is not nearly as great as for the numbers of spikes, only a 10% decrease being found as m is decreased from 15 to 7 (Fig. A2). (A decrease is expected, of course, since more spikes are being removed.) Over the period 0 to 1020 min the variance series are very much the same as in Fig. 4, except the amplitudes are higher now, i.e., the average ratio of the Fig. A1 values to those in Fig. 4 are 1.58 for the 50 m series and 1.33 at 61 m. This is consistent with the section 3 result that, for an energetic event, a variance calculated from an individual sensor with no spike removal is about 1.6 times the associated minimum variance between the two available sensors. Given the observed spike density, it is estimated that, for a large-amplitude event, at most 1% of the variance is attributable to (undetectable) spikes if each spike lasts 3 ms and has an amplitude comparable to the microstructure signal.

REFERENCES

Atlas, D., J. I. Metcalf, J. H. Richter and E. E. Gossard, 1970: The birth of "CAT" and microscale turbulence. *J. Atmos. Sci.*, **27**, 903–913.

Caldwell, D. R., 1983: Small-scale physics of the ocean. *Rev. Geophys. Space Phys.*, **21**, 1192–1205.

D'Asaro, E. A., 1985: Upper ocean temperature structure, inertial currents, and Richardson numbers observed during strong meteorological forcing. *J. Phys. Oceanogr.*, **15**, 943–962.

Desaubies, Y., and M. C. Gregg, 1981: Reversible and irreversible finestructure. *J. Phys. Oceanogr.*, **11**, 541–556.

Dillon, T. M., 1982: Vertical overturns: A comparison of Thorpe and Ozmidov length scales. *J. Geophys. Res.*, **87**, 9601–9613.

——, 1984: The energetics of overturning structures: Implications for the theory of fossil turbulence. *J. Phys. Oceanogr.*, **14**, 541–549.

——, and D. R. Caldwell, 1980: The Batchelor spectrum and dissipation in the upper ocean. *J. Geophys. Res.*, **85**, 1910–1916.

Dugan, J. P., and B. Okawa, 1982: Indirect technique for small scale temperature and salinity measurements. *Proc. Int. STD Conf. and Workshop*, La Jolla, Mar. Technol. Soc., 7 pp.

Gargett, A. E., 1978: Microstructure and fine structure in an upper ocean frontal regime. *J. Geophys. Res.*, **83**, 5123–5134.

——, and R. W. Schmitt, 1982: Observations of salt fingers in the central waters of the Eastern North Pacific. *J. Geophys. Res.*, **87**, 8017–8030.

Gibson, C. H., 1982: Fossil turbulence in the Denmark Strait. *J. Geophys. Res.*, **87**, 8039–8046.

Gregg, M. C., 1980: Microstructure patches in the thermocline. *J. Phys. Oceanogr.*, **10**, 915–943.

——, and T. B. Sanford, 1980: Signatures of mixing from the Bermuda slope, the Sargasso Sea and the Gulf Stream. *J. Phys. Oceanogr.*, **10**, 105–127.

Hayes, S. P., T. M. Joyce and R. C. Millard, 1975: Measurements of vertical fine structure in the Sargasso Sea. *J. Geophys. Res.*, **80**, 314–319.

Marmorino, G. O., L. J. Rosenblum, J. P. Dugan and C. Y. Shen, 1985: Temperature finestructure patchiness near an upper ocean density front. *J. Geophys. Res.*, **90**, 11799–11810.

Meagher, T. B., A. M. Pederson and M. C. Gregg, 1982: A low-noise conductivity microstructure instrument. *Proc. Mar. Technol. Soc./IEEE Conf. Oceans '82*, Washington DC, Mar. Technol. Soc./IEEE, 283–290.

Morris, W. D., J. P. Dugan, B. S. Okawa, C. W. Martz and E. E. Rudd, 1983: Towed thermistor system for marine research. *Proc. IEEE Third Working Symp. on Oceanographic Data Systems*, Silver Spring IEEE Computer Soc., 147–153.

Nasmyth, P. W., 1980: Towed vehicles and submersibles. *Air–Sea Interaction: Instruments and Methods*. F. Dobson, L. Hasse and R. Davis, Eds., Plenum, 739–765.

Oakey, N. S., and J. A. Elliott, 1977: Vertical temperature gradient structure across the Gulf Stream. *J. Geophys. Res.*, **82**, 1369–1380.

Okawa, B. S., and J. P. Dugan, 1984: Contamination of conductivity measurements by waterborne particles. *Ocean Eng.*, **11**, 265–279.

Padman, L., and I. S. F. Jones, 1985: Richardson number statistics in the seasonal thermocline. *J. Phys. Oceanogr.*, **15**, 844–854.

Rosenblum, L. J., G. O. Marmorino and J. P. Dugan, 1985: A processor for the study of ocean fine-scale patches. NRL Memo. Rep. 5573, Washington, DC, 44 pp.

Schertzer, D., and S. Lovejoy, 1984: The dimension and intermittency of atmospheric dynamics. *Turbulent Shear Flows 4*. L. J. S. Bradbury and co-Editors, Springer-Verlag, 7–33.

Trump, C. L., B. S. Okawa and R. H. Hill, 1985: The characterization of a midocean front with a Doppler shear profiler and a thermistor chain. *J. Atmos. Oceanic Technol.* **2**, 508–516.

Washburn, L., and C. H. Gibson, 1982: Measurement of oceanic temperature microsctructure using a small conductivity probe. *J. Geophys. Res.*, **87**, 4230–4240.

——, and ——, 1984: Horizontal variability of temperature microstructure at the base of a mixed layer during MILE. *J. Geophys. Res.*, **89**, 3507–3522.